steel research international
www.steel-research.de

Numeric Simulation of the Steel Flow in a Slab Caster with a Box-Type Electromagnetic Stirrer

Martin Barna, Mirko Javurek, and Peter Wimmer*

The usage of electromagnetic actuators in the continuous steel-casting process is on a steady rise, due to its possibilities for a sophisticated, contactless flow control. The complexity of the casting process and the ever-increasing quality demands require a well-founded knowledge of the interaction between the electromagnetic actuators and the liquid steel flow. Numeric modeling provides a detailed view and is therefore crucial for understanding the interaction between the electromagnetic fields and the liquid steel flow. Only a deep insight into the coupling between the liquid steel flow and the electromagnetic forces makes it possible to improve/optimize the continuous casting process. The work presented here is part of an ongoing research to bridge the gap between the liquid steel flow and the grain structure of the end product. The article's focus lies on the liquid steel flow modified by a traveling magnetic field—relying mainly on numerical simulations. Different modeling approaches are used to simulate linear electromagnetic stirring in the secondary cooling zone of a slab caster. An appropriate model is chosen to investigate the influence of various stirring parameters, stirring modes, and stirring positions. From the results, conclusions for the real casting process can be drawn.

1. Introduction

In the continuous casting of steel, the flow in the liquid core of the strand has a significant impact on the quality of the solidified half product, the slab. To enhance or even control the liquid steel flow, a huge number of techniques has been developed and used over time and around the world. In the last decades, the application of electromagnetic fields has become popular as a method to control/modify the flow in continuous casting of steel.[1–4] In bloom and billet casters, rotary electromagnetic fields are commonly used to impose an additional circumferential motion.[5–11]

Dr. M. Barna, Dr. M. Javurek
Institute of Fluid Mechanics and Heat Transfer
Johannes Kepler University Linz
Altenbergerstraße 69, 4040 Linz, Austria
E-mail: martin.barna@jku.at

Dr. P. Wimmer
Primetals Technologies Austria GmbH
Turmstraße 44, 4031 Linz, Austria

The ORCID identification number(s) for the author(s) of this article can be found under https://doi.org/10.1002/srin.202000067.

DOI: 10.1002/srin.202000067

In the slab casting process, mostly electromagnetic brakes are used.[12–15] Although the principle of linear electromagnetic stirring for steel slab casters is not quite new, until recently it was rarely used.[12,16,17] Special steel grades, such as ferritic stainless steels or silicon steels, and/or increasing quality demands require the usage of linear electromagnetic stirring for slab casting.[1,2,18] The traveling magnetic fields of the stirrers are often located near the mold, where they shall brake/accelerate or even stir the flow in the mold region.[19–21] Scarcer are publications, where the linear stirrer is located in the secondary cooling zone. In these cases, the stirrer shall impose an additional motion on the otherwise rather calm flow.[22,23] Dubke et al. were among the first to present a model to simulate electromagnetic stirring.[24–26] Felten et al. used this model in a Large Eddy Simulation (LES) of a shallow hexahedron to investigate the influence of the oscillating part of the Lorentz forces onto the flow.[27] El-Kaddah et al. also modeled linear stirring but in a straight section of a strand with a total height of $\approx$3.5 m.[17] They used the current vector potential and reduced magnetic scalar potential to calculate the electromagnetic forces. These publications were focused on the principle of linear stirring, as they did not take the actual geometry of the stirrer (box-type stirrer, in-roll stirrer…) nor the features of the strand geometry (curvature, solidification…) into account. Lin and Kuo compared an analytical model with numerical results from an electromagnetic simulation of in-roll stirrers.[28] Chen et al. investigated the effects of different setups of in-roll stirrers onto a straight strand, where the solidified shell was considered.[22] Gong et al. considered the curvature of the strand but neglected the solidified shell in their investigation of various in-roll stirrer setups.[29] Jiang et al. investigated the impact of electromagnetic forces produced by in-roll stirrers onto the solidification behavior in the strand.[30] In contrast to these publications, the impact of linear electromagnetic stirring produced by a box-type stirrer onto the flow in a slab caster is considered.

Plant trials and experiments are difficult or impossible to conduct, as safety guidelines etc. have to be fulfilled. Measurements are complicated because of the high temperatures and the opaqueness of liquid steel. Therefore, a numerical approach is chosen to gain a better understanding of the interaction between the transient electromagnetic field and the liquid steel flow and subsequently to optimize the stirrer together with the casting process.

2. Mathematical Model

2.1. Fluid Properties

The liquid steel is assumed a Newtonian, incompressible fluid. The liquid steel's temperature is well above the Curie temperature ($T_{\text{Curie}} = 768\,°\text{C}$) in the whole computational domain, so the liquid steel is no longer ferromagnetic.[22,31] All used material properties are assumed to be constant and are calculated/fixed for a temperature of $T = 1550\,°\text{C}$. The relevant material properties are summarized in **Table 1**.

2.2. Flow Field

The liquid steel flow in the cast strand is described by the Navier–Stokes equations; see Equation (1).

$$\nabla \cdot \boldsymbol{u} = 0,\ \frac{\partial \boldsymbol{u}}{\partial t} + (\boldsymbol{u} \cdot \nabla)\boldsymbol{u} = -\frac{1}{\rho}\nabla \boldsymbol{p} + \boldsymbol{\nu}\nabla^2 \boldsymbol{u} + \frac{1}{\rho}\boldsymbol{j} \times \boldsymbol{B} \tag{1}$$

The term $\frac{1}{\rho}\boldsymbol{j} \times \boldsymbol{B}$ describes the Lorentz forces acting on the fluid. The liquid steel flow is highly turbulent due to the high momentum of the jets exiting the submerged entry nozzle (SEN). The turbulent flow is mathematically described by the Reynolds averaged Navier–Stokes equations (RANS), using the realizable k–ε turbulence model for closure.[33]

2.3. Electromagnetic Field and Forces

For the calculation of the electromagnetic forces, two approaches are used:

In the first approach, Maxwell's equations (Equation (2)–(5)) and Ohm's law (Equation (6)) are used to describe the magnetic field and the electromagnetic forces, the so-called Lorentz forces. Due to the good electrical conductivity of liquid metals, the displacement current $\frac{\partial \varepsilon E}{\partial t}$ can be neglected in Equation (3).[34] Equation (5) can therefore be omitted.[34]

$$\nabla \times \boldsymbol{E} = -\frac{\partial \boldsymbol{B}}{\partial t} \tag{2}$$

Here, $\boldsymbol{E}$ is the electric field and $\boldsymbol{B}$ the magnetic flux density.

$$\nabla \times \boldsymbol{H} = \boldsymbol{J} + \frac{\partial \varepsilon \boldsymbol{E}}{\partial t} \tag{3}$$

The symbol $\boldsymbol{H}$ stands for the magnetic field, $\boldsymbol{J}$ for the eddy current density, and ε for the electrical permittivity.

Table 1. Liquid steel properties.

		Liquid steel ($T = 1550\,°\text{C}$)
Density, ρ	kg m^{-3}	7044
Dynamic viscosity, μ	$\text{kg m}^{-1}\,\text{s}^{-1}$	0.0060
Kinematic viscosity, ν	$\text{m}^2\,\text{s}^{-1}$	8.5×10^{-7}
Electrical conductivity, σ_{Liquid}[29,32]	S m^{-1}	0.714×10^6
Relative permeability, $\mu_{\text{M,r}}$	–	1

$$\nabla \cdot \boldsymbol{B} = 0 \tag{4}$$

$$\nabla \cdot \varepsilon \boldsymbol{E} = 0 \tag{5}$$

In addition, Ohm's law and rules for the material behavior are needed. A linear connection between the magnetic flux density $\boldsymbol{B}$ and the magnetic field strength $\boldsymbol{H}$ is assumed. Any saturation effects are not considered. Although this may not prove true for the iron core of an electromagnetic stirrer, the assumption will hold for the electromagnetic field inside the strand.

$$\boldsymbol{J} = (\boldsymbol{E} + \boldsymbol{u} \times \boldsymbol{B}) \tag{6}$$

$$\boldsymbol{B} = \mu_M \boldsymbol{H} \tag{7}$$

Equation (2)–(4), (6), and (7) can be transformed into the induction equation (see Equation (8)). An alternative formulation uses the magnetic vector potential $\boldsymbol{A}$ instead of the magnetic flux density $\boldsymbol{B}$, which leads to Equation (9). It has the benefit of implicitly guaranteeing the solenoidality of the magnetic flux density, because $\nabla \cdot \boldsymbol{B} = \nabla \cdot (\nabla \times \boldsymbol{A}) = 0$ will always be fulfilled.

$$\frac{\partial \boldsymbol{B}}{\partial t} + (\boldsymbol{u} \cdot \nabla)\boldsymbol{B} = \frac{1}{\mu_M \sigma}\Delta \boldsymbol{B} + (\boldsymbol{B} \cdot \nabla)\boldsymbol{u} \tag{8}$$

$$\frac{\partial \boldsymbol{A}}{\partial t} = \frac{1}{\mu_M \sigma}\Delta \boldsymbol{A} + \boldsymbol{u} \times (\nabla \times \boldsymbol{A}) \tag{9}$$

The electromagnetic forces $\boldsymbol{F}$ can then be calculated from the eddy current density $\boldsymbol{J}$ and the magnetic flux density $\boldsymbol{B}$ (following Equation (10)) and inserted into the Navier–Stokes equations as a volumetric force.

$$\boldsymbol{F} = \boldsymbol{J} \times \boldsymbol{B} \tag{10}$$

This approach allows the calculation of the electromagnetic forces on the fluid for an arbitrary flow field. Nevertheless, the computational effort in a transient flow simulation is too high. Therefore, a second approach for the calculation of the electromagnetic forces is considered. Dubke et al. also started from Maxwell's equations and developed a mathematical model for linear stirring of a half-infinite fluid region.[24–26] An analytical, harmonic solution can be found for the case of a resting fluid. This solution is semi-empirically enhanced to account for the difference between the velocity of the traveling electromagnetic field, given by $v_{\text{sync}} = \omega \cdot \lambda^{-1}$, and the liquid steel flow (see Equation (11) and (12)).

$$\langle F_x \rangle_t = \frac{\sigma(\omega - v_x \lambda)}{2\lambda} B_0^2 e^{-2\mathfrak{Re}\{\gamma y\}} \tag{11}$$

$$\langle F_y \rangle_t = \frac{\sigma(\omega - v_x \lambda)}{2\lambda^2} B_0^2 \mathfrak{Im}\{\gamma\} e^{-2\mathfrak{Re}\{\gamma y\}} \tag{12}$$

with

$$\gamma = \sqrt{\sigma \mu_{\text{M}} \omega i + \lambda^2} \tag{13}$$

In these equations, γ describes the damping of the magnetic field perpendicular to the strand wall and is formed by the electrical conductivity σ, the magnetic permeability μ_{M}, the angular frequency $\omega = 2 \cdot \pi \cdot f$ (with f being the stirring frequency) and the wave number λ, which is proportional to the inverse of the pole pitch $\lambda = \pi \cdot \tau^{-1}$. The magnetic permeability μ_M is the product of the permeability of vacuum $\mu_{0,M}$ and the relative permeability $\mu_{\text{rel},M}$. The symbol i signifies the imaginary unit and the symbols $\mathfrak{Re}\{\}$ and $\mathfrak{Im}\{\}$ label the real part respectively the imaginary part of the complex number within the brackets. With this second approach, neither the magnetic field nor the eddy current distribution in the strand is explicitly calculated, only the resulting Lorentz forces. These forces are then time-averaged over one period $T = f^{-1}$ leading to the forms shown in Equation (11) and (12).

As in most industrial processes, the magnetic Reynolds number is smaller than 1.[34,35] This means that magnetic diffusion is stronger than magnetic convection and the liquid steel flow only has a small effect on the magnetic field. The Hartmann number Ha, which is the ratio of electromagnetic forces to the viscous forces, is around 200.[34,35] It means that the electromagnetic forces have a significant impact on the liquid steel flow. Finally but also importantly, the Stuart number (also known as the interaction parameter) combines the Hartmann number and the Reynolds number. It is smaller than 1, meaning the magnetic forces are small compared to inertial forces.[34,35]

3. Numerical Model

The numerical solution process is split into two parts. The first part is the calculation of the electromagnetic field and the Lorentz forces. The second part is the simulation of liquid steel flow considering the Lorentz forces. Each part uses its own solver as well as its own model/mesh. The two meshes differ significantly from one another, in terms of geometry and in the local mesh resolution, as will be detailed later. Consequently, the number of elements/cells also varies for the two meshes, about 0.7 million elements for the electromagnetic mesh and about 1.8 million cells for the flow simulation.

3.1. Magnetic Field and Lorentz Forces

An electromagnetic model is implemented in ANSYS EMAG to calculate the electromagnetic field inside the strand for a fluid at rest—using the first approach described earlier. The box-type stirrer (part 2 and 3 in **Figure 1**b) is modeled together with a section of the strand (part 1 in Figure 1b). The strand is divided into the solidified shell and the liquid core as shown in Figure 1a. The supporting rolls are also modeled to account for any shielding effects of the magnetic field. A shielding effect occurs if an electrically conducting body (the shielding object) is placed between the source of the electromagnetic field (the stirrer) and the liquid core of the strand (the target). Eddy currents are induced in the shielding object, accompanied by their own magnetic field. This secondary magnetic field opposes the stirring field, thereby dampening it. The shielding effect increases with the stirring frequency, the conductivity of the shielding object, etc.

A box-shaped air volume (not shown in Figure 1) encloses the whole model. The edge-based formulation of Equation (9) is used in ANSYS EMAG to perform a harmonic simulation at stirring frequency.[36] In the simulation, the traveling magnetic field is produced by imposing a three-phase current in the stirring coils, defined by the eddy current density amplitude, each coil's phase angle and the stirring frequency. The direction of the traveling field is indicated in Figure 1b by a red arrow (position 4). Another red arrow (position 6) indicates the corresponding direction of the generated fluid flow. The magnetic flux density is also shown schematically in Figure 1b.

For the second approach (the semi-empirical model), a magnetic flux density amplitude must be provided (B_0 in Equation (11) and (12)). Here, the maximum flux density amplitude in the center of the stirrer at the outer solidification front from the electromagnetic model is chosen. The extent of the stirrer's region of influence is set such that the total Lorentz forces acting on the resting liquid steel match with those calculated by the electromagnetic solver. Therefore, the magnetic field, which is calculated just once at the beginning, is not influenced by the liquid steel flow. But the Lorentz forces are scaled according to the velocity difference between the liquid steel flow and the traveling magnetic field, as described earlier.

3.2. Flow Field

For the flow simulation, the whole strand with a cross section of 1550 mm × 215 mm and a casting speed 1.1 m min^{-1} is

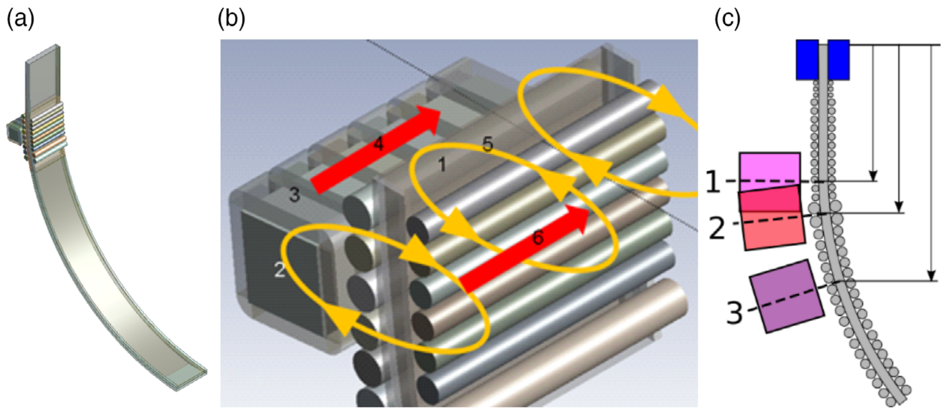

Figure 1. a) Overview of the whole strand with stirrer and support rolls. b) Detailed view of the box-type stirrer and the strand section used in ANSYS EMAG. C) Positions of the box-type stirrer along the strand.

modeled down to a metallurgical length of nearly 15 m (Figure 1a,c). The curvature of the strand and the reduction of the liquid domain due to solidification are considered. The solidification front is modeled as a wall, whose shape is calculated a priori with a shell thickness increasing proportional to the square root of the distance to the meniscus. Sink terms at the wall adjacent computational grid cells consider the material loss due to solidification.[37] The computational grid has boundary layers with 0.3 mm initial thickness and these are combined with the enhanced wall treatment to resolve the flow boundary layer.[38] Geometric symmetries are not utilized, to resolve possible asymmetrical flow fluctuations.

For the calculation of the Lorentz forces acting on the liquid steel flow, only the semi-empirical model is used, as the computational effort for a fully coupled simulation would be far too high. Therefore, the Lorentz forces described by Equation (11) and (12) are implemented in a user-defined function (UDF) in Ansys Fluent. The liquid steel flow is resolved by steady and transient simulations.

4. Results

The first step in the investigation is a closer look at the electromagnetic model. With the results and the gained insight, the stirrer model was refined stepwise for subsequent simulations. In the initial model (with a straight strand), a conducting contact between the support rolls and the strand was assumed. Due to the higher electrical conductivity of the rolls $\sigma_{\text{Rolls}} = 1.450\ \text{MS m}^{-1}$—compared with the conductivity of the solidified shell $\sigma_{\text{Shell}} = 0.800\ \text{MS m}^{-1}$, respectively, the liquid core $\sigma_{\text{Liquid}} = 0.714\ \text{MS m}^{-1}$—the eddy currents induced in the rolls will be higher than those in the strand. In the contact area, high eddy currents flow between the support rolls and the solidified strand. The developing eddy current circulation differs from the case where the strand is not in contact with the support rolls. This, in turn, affects also the Lorentz force distribution (compare **Figure 2**b and **3**). At the real process, the electrical contact between support rolls and strand will be far from perfectly conducting, due to slack powder sticking to the strand, scale formation, cooling water, etc. To account for these situations, simulations without electrical contact between the support rolls and the strand are performed: one, where the support rolls are assumed conducting and one, where they are assumed nonconducting. The results indicate if and how the support rolls are influencing the eddy currents and Lorentz force distribution in the strand.

Figure 4 shows the eddy current distribution in the support rolls and the strand for the setups with conducting and nonconducting support rolls (both times without contact between strand and support rolls). Compared with the eddy currents induced in the strand, those in the support rolls are about 44% higher. Nevertheless, the shielding effect due to these high eddy currents is negligible, as shown in Figure 4b.

In the present case, neither a qualitative nor a quantitative deviation between the two cases can be seen. Figure 3 shows

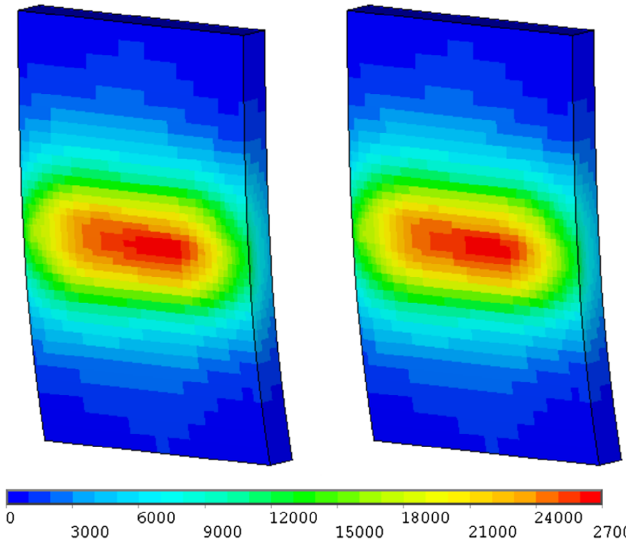

Figure 3. Comparison of Lorentz force distribution (in N m^{-3}) for nonconducting rolls (left) and electrically conducting rolls (right); only the strand is shown.

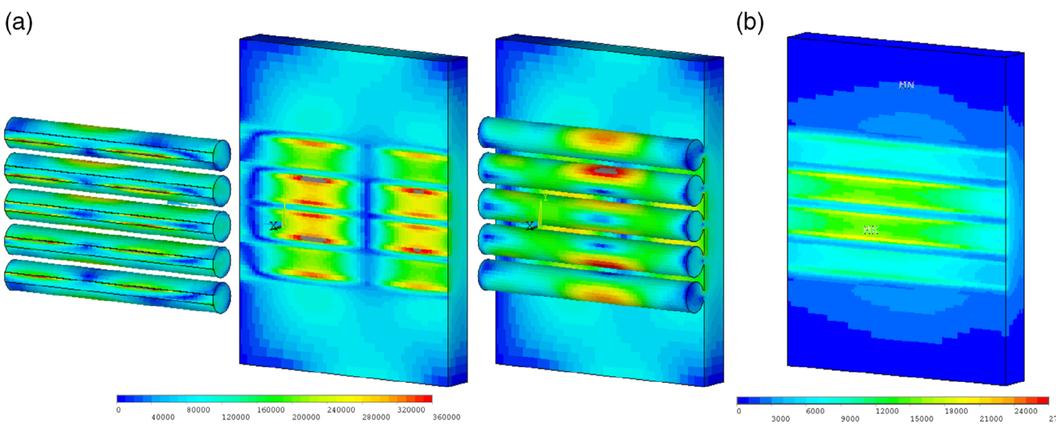

Figure 2. a) Eddy current distribution (in A m^{-2}) for the setup with conducting support rolls in perfect contact with the strand; the contact area of support rolls and strand are shown in the left and middle graphic; b) Lorentz force distribution (in N m^{-3}) in the strand for the setup with perfect contact between support rolls and strand.

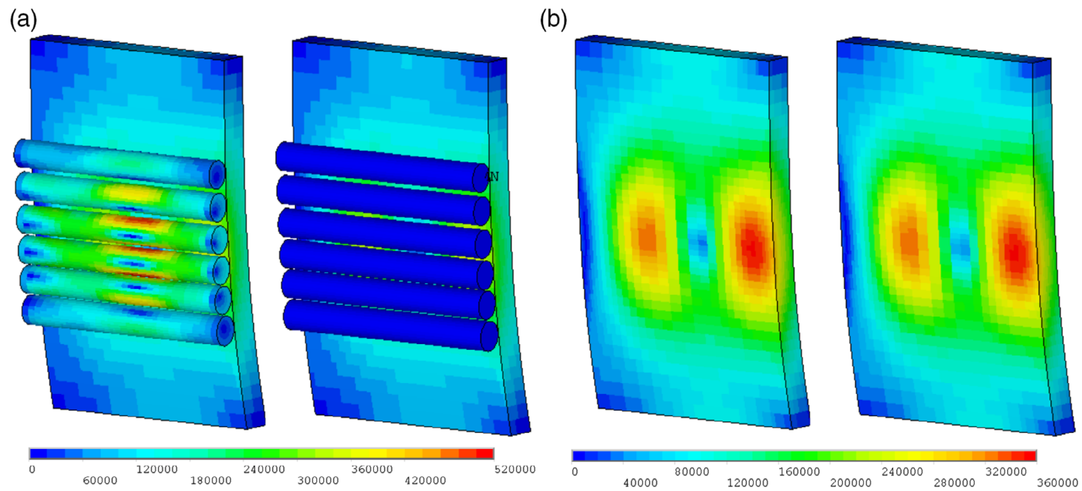

Figure 4. Comparison of eddy current distribution (in A m^{-2}) for electrically conducting support rolls and nonconducting rolls; a) strand (shell and liquid core) and support rolls are shown; b) only strand is shown.

the Lorentz force distribution at the strand surface (next to the stirrer). Again, no difference between the two cases can be seen.

In summary, the decision how the electrical contact between support rolls and strand is modeled, has the biggest impact on the Lorentz force distribution. The contact resistance occurring in the real casting process cannot be clearly defined, but it will probably be rather high due to the reasons mentioned earlier. In this model, an infinitely high contact resistance was assumed, effectively separating the support rolls and the strand electrically.

Figure 5–7 show an exemplary result of the harmonic simulation for the electromagnetic calculation at the outer solidification front, which is nearest to the box-type stirrer, the middle plane of the strand, and the inner solidification front. These results were calculated for a liquid steel at rest.

The magnetic flux density distribution is plotted in Figure 5. In the model developed by Dubke et al., the magnetic flux density decreases exponentially with increasing distance from the stirrer. Qualitatively, the same tendency can be seen in the results from the numerical model, though the magnetic flux distribution should be more accurate as less modeling assumptions (semi-infinite strand...) had to be made in comparison to the model of Dubke et al. The magnetic flux density (Figure 5) distribution resembles a dipole arrangement, where the magnetic fields, imposed by the stirrer, enters the strand near the right narrow side and the "sink", where the magnetic field closes back to the stirrer, is located near the left narrow side. This magnetic field pattern moves along the width of the strand with the stirring velocity described earlier. At the top and the bottom of the electromagnetic model, the flux density distribution is tangential to the boundary without any significant distortion of the field. This insinuates that the vertical size of the electromagnetic model was chosen large enough to capture the stray field.

Figure 6 shows an instantaneous eddy current distribution resulting from the flux density distribution in Figure 5. As shown for the magnetic flux density, the strength of the eddy currents decreases with the distance to the stirrer. The maximum eddy

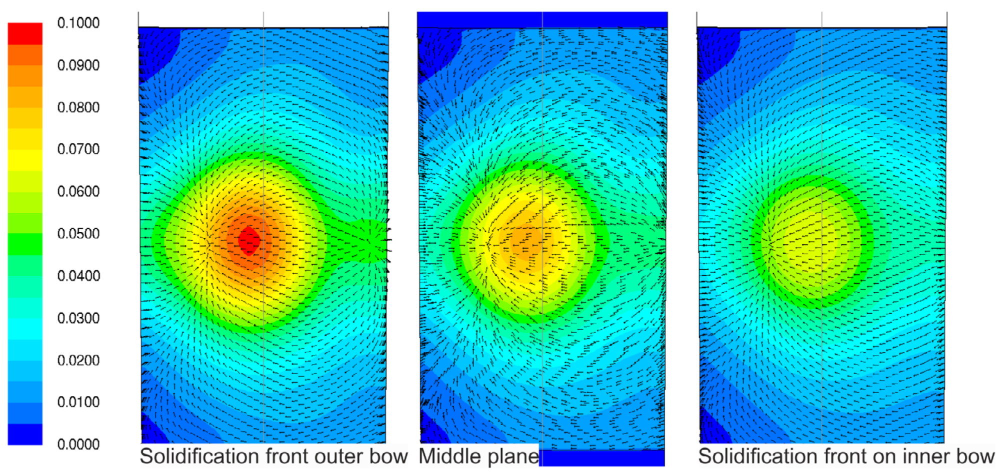

Figure 5. Contour plot with overlaid uniform vectors for an exemplary simulation result; the magnetic flux density (in T) is shown at the outer shell, center plane, and inner shell for the coupled section; the locations of the vectors do not represent the actual mesh resolution.

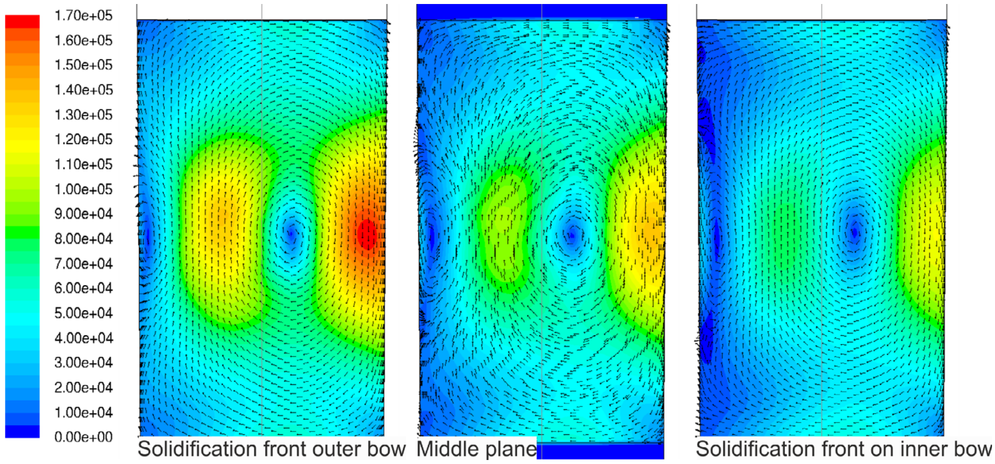

Figure 6. Contour plot with overlaid uniform vectors for an exemplary simulation result; the eddy current density (in A m^{-2}) is shown at the outer shell, center plane, and inner shell for the coupled section (black-rimmed region); the locations of the vectors do not represent the actual mesh resolution.

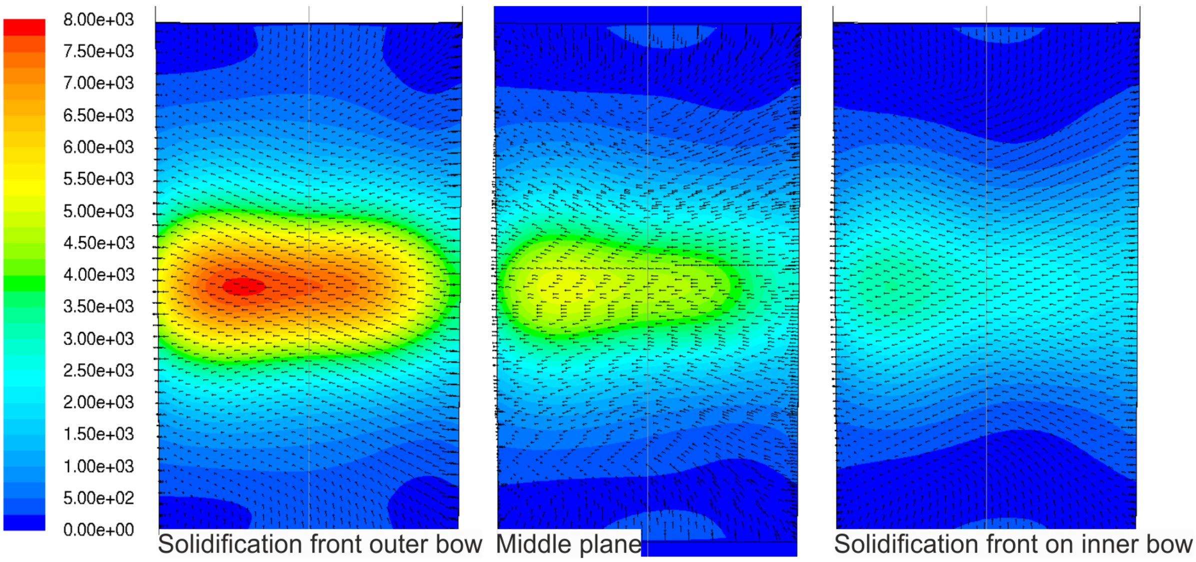

Figure 7. Contour plot with overlaid uniform vectors for an exemplary simulation result; time-averaged Lorentz force density (in N m^{-3}) at the outer shell, center plane, and inner shell for the coupled section (black-rimmed region); the locations of the vectors do not represent the actual mesh resolution.

currents occur near the right narrow face. It is 170 kA m^{-2} at the outer solidification front and only about 115 kA m^{-2} at the inner solidification front. This equals a reduction of about 32% within only 0.144 m. Due to the insulating boundary conditions at the outer shape of the solidified strand, the eddy currents have to close inside the domain, leading to an eddy vortex with the axis perpendicular to the solidification front. The center of the vortex is slightly off to one side. This shift is caused by shielding effects due to the support rolls resp. the solidified shell, which also has a slightly higher electrical conductivity than the liquid.

Following Equation (10), the cross product of the eddy current distribution and the magnetic flux density gives the Lorentz forces in the strand. Figure 7 shows a vector-plot of the Lorentz forces, time-averaged over one period of the harmonic stirring field. The maximum stirring force occurs near the middle plane of the stirrer and as before decays throughout the strand (about 7800 N m^{-3} to 3263 N m^{-3}, equaling ≈42% of the maximum). Although the stirring force is the main component of the Lorentz forces, the other components cannot be neglected. All vectors in Figure 7 are normalized to see the direction of the forces far from the maximum. In these regions, the Lorentz forces are pointing toward the stirrer's middle plane, but are rather small compared to the maximum.

For the flow simulations of the whole strand, the semi-empirical model (Equation (11) and (12)) is used to conduct various flow simulations: steady and transient mode; without and with linear electromagnetic stirring; at three different positions (Figure 1c) and with varying stirring intensities and operation modes (constant and periodically alternating direction). The results are used to analyze the influence of the stirrer on the liquid steel flow.

In the first simulations, the impact of different stirring intensities on the flow field under steady stirring conditions (unidirectional stirring) is analyzed. **Figure 8**a shows the typical double vortex flow structure induced by the stirrer. As assumed, the flow velocities are increasing with the field intensity. Figure 8b shows close-ups of the mold region: Even for a mild stirring with 60% of nominal flux density, the mold flow pattern already seems to be influenced by the stirrer, and for 80% and 120% the flow pattern becomes very asymmetric due to the strong influence of the stirrer on the mold flow. In these cases, the stirring effect near the stirrer may be satisfying, but the asymmetric mold flow will probably be inacceptable and might lead to quality problems such as, e.g., mold slag entrainment. Therefore, the common praxis of periodically alternating the stirring direction is investigated next.

Figure 9 shows the resulting flow field time-averaged over a period of $T = 600$ s, whereas the traveling direction of the magnetic field is flipped every 15 s for four different cases: without and with stirring in the secondary cooling zone at three different positions (see Figure 1c). At the two lower positions, the stirring intensity is increased, as the distance from the mold level is higher. Now, in all cases, the velocity field in the mold region seems uninfluenced by the stirrer. In the region of the stirrer, the time-averaged flow velocity in Figure 9a is comparably low to the unidirectional results in Figure 8a, as the flow velocities are in large part extinguished by the stirring direction changes in combination with the time-averaging procedure. In contrast, the fluctuation velocities in Figure 9b are significantly higher in the region of the

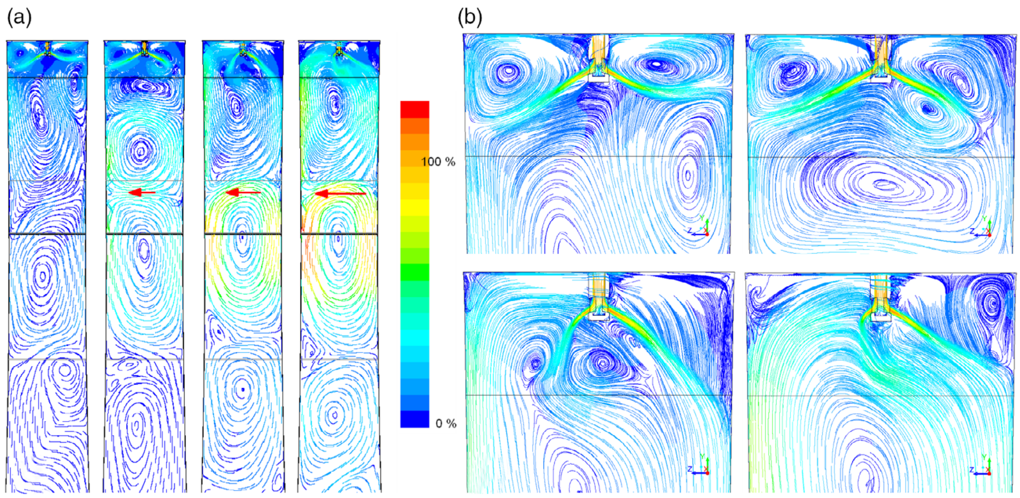

Figure 8. Velocity field in the center plane visualized by path lines colored with the velocity magnitude (color scale in percentage of the entry nozzle flow velocity) for different stirring intensities (from left to right: magnetic field 0%, 60%, 85%, 120% of nominal flux density); results from steady flow simulations with unidirectional stirring; a) overview, red arrows denote stirrer position and force direction; b) close-ups of the mold region.

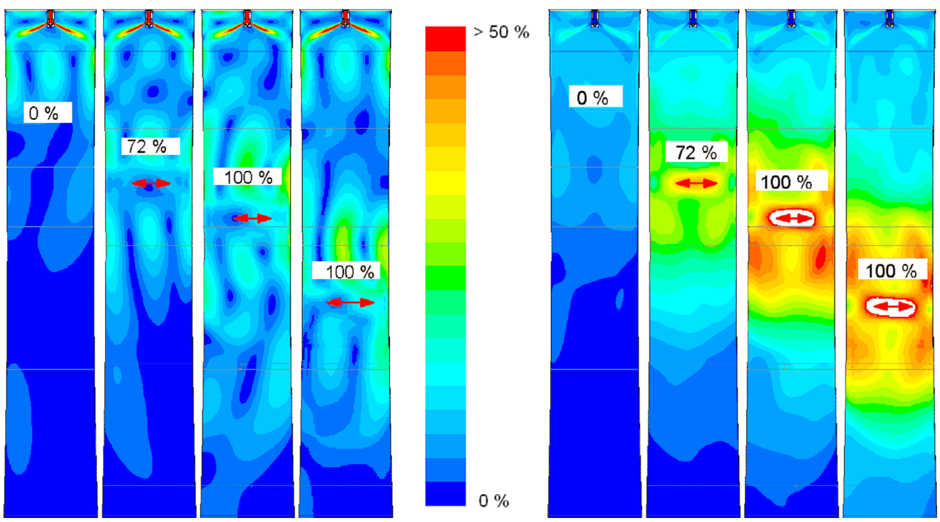

Figure 9. a) Mean velocity magnitude and b) mean velocity deviations (mean of the fluctuation velocity magnitude) in the center plane of the strand from transient simulations with periodically alternating stirring direction and varying stirrer positions and intensities (in percentage of nominal flux density); arrows denote the stirrer positions, the color scale (in percentage of the entry nozzle flow velocity) is the same for both pictures.

stirrer (approximately within ±2 m above and below the stirrer) than without stirring.

5. Conclusion

A simulation model of a linear electromagnetic stirrer was used to investigate the influence of the support rolls onto the Lorentz force distribution inside the strand. The support rolls have a higher electrical conductivity than the solidified shell and the liquid core of the strand. The results show that the contact condition between the strand and the rolls has the biggest impact. A perfect electrical contact leads to eddy currents flowing through the small contact area between shell and rolls. Thus, the Lorentz forces inside the strand are dampened. If, on the other hand, no contact between rolls and strand is assumed, no shielding effect can be observed. As the contact condition (conductivity and contact area) between strand and shell is not known and rather complex to model, a no-contact condition is assumed for subsequent simulations.

With the results from the electromagnetic model, various simulations of the liquid steel flow of a continuous casting process are conducted. The Lorentz forces are calculated with the approach of Dubke et al. in combination with the numerical electromagnetic model. The influence of different vertical positions, magnetic field intensities, and operating modes (unidirectional stirring, periodically alternating stirring direction) is investigated. The results show that an alternating stirring direction is essential to avoid a probably unfavorable impact of the stirring on the mold flow, while still maintaining a strong enough movement of the liquid steel in the bending zone of the strand. The region influenced by the stirring extents about one strand width above and below the stirrer center position. The velocity fluctuation intensity in this region is significantly higher than in the mold region.

Despite the thicker solidified shell in the lower stirring positions, the stirring effect is still higher due to the (arbitrarily) increased imposed magnetic field density. Therefore, magnetic field densities lower than considered will reach the same stirring intensities in the lower positions in comparison to the uppermost stirrer position.

A further important aspect not considered here is the relation between the electromagnetically stirred liquid steel velocities and the resulting steel quality. Some attempts for such considerations are published by Javurek et al.[39]

Acknowledgements

The authors gratefully acknowledge the funding support of K1-MET GmbH, Metallurgical Competence Center. The research program of the K1-MET Competence Center is supported by COMET (Competence Center for Excellent Technologies), the Austrian program for competence centers. COMET is funded by the Federal Ministry for Transport, Innovation and Technology, the Federal Ministry for Digital and Economic Affairs and the provinces of Upper Austria, Tyrol and Styria. In addition to the public funding from COMET, this research project is partially financed by the industrial partner Primetals Technologies Austria GmbH.

Conflict of Interest

The authors declare no conflict of interest.

Keywords

computational fluid dynamics, continuous casting, linear electromagnetic stirring, numeric simulations, slabs, steels

Received: February 8, 2020
Revised: July 16, 2020
Published online: August 9, 2020

[1] S. Kunstreich, *La Rev. Métallurgie-CIT* **2003**, *100*, 395.
[2] S. Kunstreich, *La Rev. Métallurgie-CIT* **2003**, *100*, 1043.
[3] B. G. Thomas, S. M. Cho, *IOP Conf. Ser. Mater. Sci. Eng.* **2018**, *424*, 012027.
[4] S. Cho, B. G. Thomas, *Metals (Basel)* **2019**, *9*, 38.
[5] L. S. Beitelman, *ISIJ Int.* **2005**, *45*, 142.
[6] F.-C. Chang, J. R. Hull, L. S. Beitelman, in *Proc. 78th Steelmaking Conf. 53rd Ironmaking Conf.*, Iron & Steel Society, Nashville, **1995**, p. 26.
[7] T. Toh, H. Hasegawa, H. Harada, *ISIJ Int.* **2001**, *41*, 1245.
[8] H. Harada, T. Toh, T. Ishii, K. Kaneko, E. Takeuchi, *ISIJ Int.* **2001**, *41*, 1236.
[9] H. K. Moffatt, in *Second Bat-Sheva International Seminar* (Eds.: H. Branover, A. Yakhot), Cambridge University Press, Beersheva **1978**, pp. 45–62.
[10] O. Peşteanu, K. Schwerdtfeger, *ISIJ Int.* **2003**, *43*, 1556.
[11] K.-H. Spitzer, *Berechnung von Strömungen Beim Elektromagnetischen Rotationsrühren von Rundsträngen*, Technische Universität Clausthal, Clausthal-Zellerfeld **1985**.
[12] H. Yamamura, T. Toh, H. Harada, E. Takeuchi, T. Ishii, K. Kaneko, *ISIJ Int.* **2001**, *41*, 1229.
[13] Y. Haiqi, W. Baofeng, L. Huiqin, L. Jianchao, *J. Mater. Process. Technol.* **2008**, *202*, 179.
[14] Y. Wang, L. Zhang, in *AISTech 2009*, Curran Associates, Inc., St. Louis **2009**, pp. 559–572.
[15] R. Chaudhary, B. G. Thomas, S. P. Vanka, *Metall. Mater. Trans. B* **2012**, *43*, 532.
[16] N. Kubo, T. Ishii, J. Kubota, T. Ikagawa, *ISIJ Int.* **2004**, *44*, 556.
[17] N. El-Kaddah, T. T. Natarajan, P. Industries, in *Proc. Second Int. Conf. CFD Miner. Process Ind. CSIRO*, CSIRO, Melbourne **1999**, pp. 339–344.
[18] V. Lambert, J. M. Galpin, H. R. Hackl, N. P. Jacobson, *Iron Steel Technol.* **2008**, *5*, 71.
[19] S. Kunstreich, T. Gautreau, J. Y. Ren, A. Codutti, F. Guastini, M. Petronio, *Milen. Steel* **2015**, *8*, 86.
[20] S. Kunstreich, *Millenn. Steel* **2014**, *11*, 57.
[21] J. Nakashima, J. Fukuda, A. Kiyose, T. Kawase, Y. Ohtani, M. Doki, *Improvement of Slab Surface Quality with Ln-Mold Electromagnetic Stirring*, Nippon Steel Corporation, Tokyo **2002**.
[22] J. Chen, S. Lin, M. Lu, *Process Simulation of S-EMS and Its Application in Slab Continuous Casting*, China Steel Corp., Kaohsiung, Taiwan **2010**.
[23] K. Okazawa, T. Toh, J. Fukuda, T. Kawase, M. Toki, *ISIJ Int.* **2001**, *41*, 851.
[24] M. Dubke, *Untersuchung Der Strömung Beim Linearen Rühren von Stahlstrangguss*, TU Clausthal-Zellerfeld, Clausthal-Zellerfeld **1985**.
[25] M. Dubke, K. H. Tacke, K. H. Spitzer, K. Schwerdtfeger, *Metall. Trans. B* **1988**, *19*, 581.
[26] M. Dubke, K. H. Tacke, K. H. Spitzer, K. Schwerdtfeger, *Metall. Trans. B* **1988**, *19*, 595.

[27] F. Felten, Y. Fautrelle, Y. Du Terrail, O. Metais, *Appl. Math. Model.* **2004**, *28*, 15.
[28] S. Lin, S. Kuo, *Electromagnetic Force Predictions of a Stand Electromagnetic Stirring System Using an Analytical Model*, China Steel Corp., Kaohsiung, Taiwan **2008**.
[29] J. Gong, H. P. Liu, X. H. Wang, Y. P. Bao, *J. Iron Steel Res. Int.* **2015**, *22*, 414.
[30] D. Jiang, M. Zhu, L. Zhang, *Metals* **2019**, *9*, 452.
[31] BDS AG – Bundesverband Deutscher Stahlhandel, Kerschgens Stahllexikon, https://kerschgens.stahl-lexikon.de/index.php/stahllexikon/37-c/1332-Curie-Temperatur.html (accessed: May 2020).
[32] V. Goman, I. Sokolov, S. Fedoreev, in *2019 Int. Conf. Industrial Engineering, Applications and Manufacturing ICIEAM*, IEEE, Piscataway, NJ **2019**, pp. 1–5.
[33] T.-H. Shih, W. W. Liou, A. Shabbir, Z. Yang, J. Zhu, *Comput. Fluids* **1995**, *24*, 227.
[34] R. Moreau, *Magnetohydrodynamics*, Springer-Science+Business Media, B.V., Dordrecht **2015**.
[35] P. A. Davidson, *An Introduction to Magnetohydrodynamics*, Cambridge University Press, Cambridge **2007**.
[36] ANSYS Inc., *ANSYS Mechanical APDL Theory Reference*, SAS IP, Inc, Canonsburg **2011**.
[37] M. Javurek, P. Gittler, R. Rössler, B. Kaufmann, H. Preßlinger, *Steel Res. Int.* **2005**, *76*, 64.
[38] ANSYS Inc., *ANSYS Fluent Theory Guide 19.0*, Ansys Inc., Canonsburg **2018**.
[39] M. Javurek, M. Barna, P. Wimmer, in *Proc. European Stainless Steel Conf. DUPLEX*, **2019**, p. 12.